https://doi.org/10.1038/s44384-026-00077-2

Vehicle pass-by measurements in simplified roadside wall configurations

Check for updates

Chalotorn Möhlmann ✉, Lukas Aspöck & Janina Fels

Urban traffic noise is not only dependent on the source but also on the environment. This is not explicitly represented in standardized measurement procedures such as the Statistical Pass-By (SPB) method, which captures pass-by noise without urban structures. This study investigates vehicle pass-by noise with simplified roadside wall configurations. The experimental design builds on the SPB method and introduces two roadside walls, forming single- and two-wall configurations at four receiver positions. This allows investigation of the contributions of direct, reflected, and diffracted sound. Pass-by measurements of two passenger vehicles (diesel sedan and battery-electric SUV) were repeated at speeds of 10, 30, and 50 km/h. Shadow-zone boundaries segmented each pass-by event. The analysis combines level-based indicators with the psychoacoustic metrics loudness and sharpness. Results show that the two-wall configuration has a limited influence on maximum pass-by levels (up to +3.4 dB(A) at 30 km/h and within ±1 dB(A) at 50 km/h), while primarily producing frequency-dependent spectral redistribution and differences in level, loudness, and sharpness, particularly within the shadow-zone sections. Discrepancies in the shadow zones indicate that the standardized method of analysis does not capture the full scale of perceptual investigations. The dataset provides real-track measurements for validating traffic-noise auralizations and urban propagation models.

According to the World Health Organization, road traffic noise causes adverse health effects[1]. At the same time, ongoing urbanization increases the share of the population living in urban environments where traffic noise exposure is prevalent[2]. Survey-based evidence further identifies road traffic as a major contributor to environmental noise annoyance[3].

Noise mitigation measures may reduce emissions at the source, influence sound propagation, or reduce exposure at the receiver. In urban environments, the sound propagation pathway is strongly affected by surrounding structures, which cause reflection and diffraction and can substantially alter the received sound field[4]. Diffraction denotes the bending of sound around edges and structures and can dominate when the direct line of sight between source and receiver is obstructed.

Perceptual research on road traffic noise, such as the work by Oehme et al.[5], shows that listener response depends strongly on contextual and structural factors beyond sound pressure level. However, such studies operate at a more abstract perceptual level and do not address the controlled physical interpretation of sound propagation or the use of measurements for validating auralizations and numerical traffic noise models.

Measurement data representing realistic urban sound propagation conditions are essential to capture the effects of reflection and diffraction in complex street environments. However, standardized traffic noise measurement procedures primarily aim to characterize vehicle emission—especially tire–road interaction—under controlled, quasi-free-field conditions, and therefore do not explicitly capture the influence of nearby urban structures on vehicle pass-by noise[6,7].

Prediction models for road traffic noise are well established and widely applied in environmental acoustics, for example in the context of strategic noise mapping based on the CNOSSOS-EU framework[8,9]. These regulatory engineering models commonly separate vehicle emission from outdoor sound propagation. This separation provides a practical and computationally efficient framework, but requires simplified source representations and parameterized descriptions of propagation effects such as screening and reflection. Consequently, the transient, geometry-dependent interaction between a moving vehicle and nearby urban structures may not be represented in full detail[8]. Controlled, time-resolved pass-by measurement data with systematically varied roadside geometries remain limited, particularly those that support the geometry-based interpretation of transient shielding, reflection, and diffraction effects.

In recent years, research on urban traffic noise has increasingly emphasized the need for validation of prediction and auralization models under realistic sound propagation conditions. While the physical generation mechanisms of vehicle and tire–road noise are well documented[10–12], these

Institute for Hearing Technology and Acoustics, RWTH Aachen University, Aachen, Germany. ✉e-mail: chalotorn.moehlmann@akustik.rwth-aachen.de

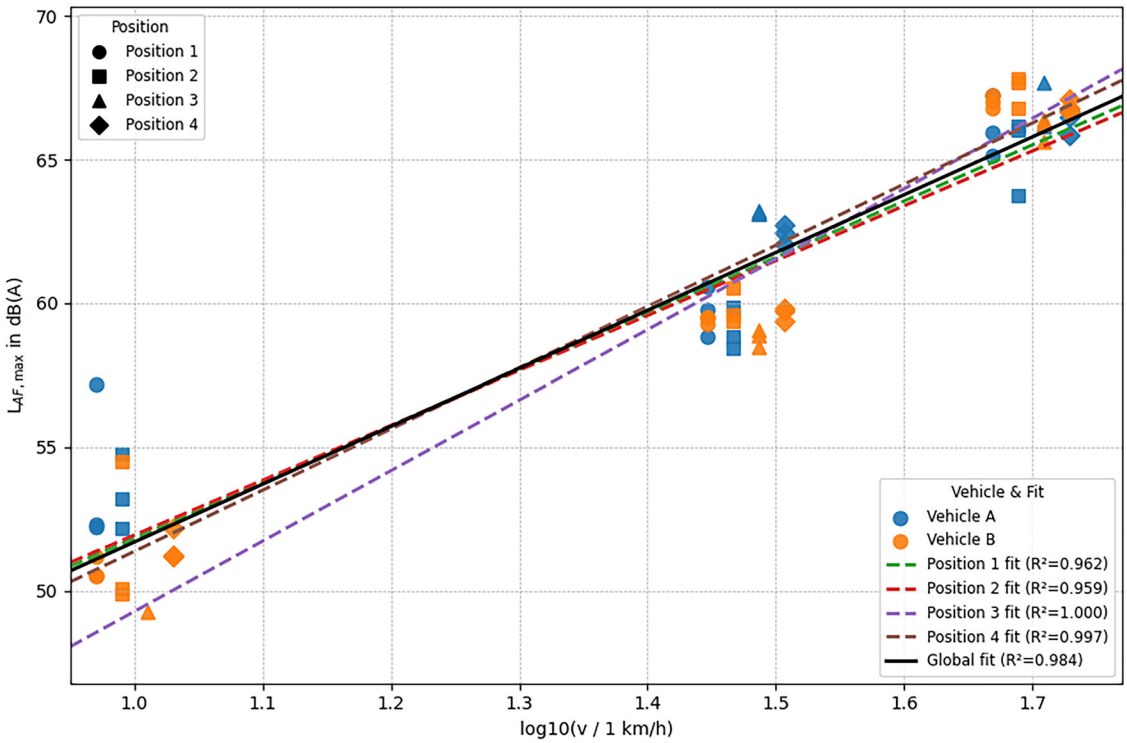


Fig. 1 | Maximum A-weighted sound pressure level $L_{AF,\max}$ versus $\log_{10}(v)$ for Vehicle A (blue) and Vehicle B (orange) based on pass-by measurements at four receiver positions $p \in \{1, 2, 3, 4\}$ (see Fig. 6). Regression fits according to Eq. (3) are shown as dashed lines for each p and as a solid line based on measurements from all positions.

studies focus primarily on source characteristics and provide limited insight into how surrounding structures influence the sound propagation of vehicle pass-by noise.

Auralization-based studies of urban traffic noise likewise rely on accurate representations of sound propagation. Georgiou et al.[13] investigated discretized vehicle pass-by representations using simulated impulse responses in simplified urban scenarios and showed that source discretization can influence the perceived pass-by. A subsequent study incorporated measured impulse responses from a real urban canyon[14]. However, such real-environment configurations do not permit systematic isolation or parameterization of individual sound propagation paths. Consequently, these studies remain primarily perceptual and do not provide controlled pass-by measurements for validating sound propagation effects.

Standardized measurement methods, including the Statistical Pass-By (SPB) method[6], the Close Proximity method[7], and acceleration noise measurements according to[15], are designed to minimize environmental propagation influences, typically by approximating free-field conditions over a reflecting plane without nearby structures affecting the measured sound field. By design, these procedures do not capture complex urban propagation effects, and the varying contributions of reflected and diffracted sound cannot be interpreted separately in the measurements.

Meanwhile, perceptual responses play a central role in the evaluation of urban traffic noise and are influenced by characteristics of the urban environment[3,5]. Existing studies do not systematically investigate how roadside wall configurations influence vehicle pass-by noise measurements or how they support the interpretation of direct, reflected, and diffracted sound path contributions[13,14]. Consequently, current measurement data are insufficient for validating models intended to predict and auralize urban traffic noise.

This study investigates how simplified roadside wall configurations affect the time-dependent and spectral characteristics of vehicle pass-by noise by altering the relative contributions of direct, reflected, and diffracted sound under controlled conditions. To this end, controlled pass-by measurements based on SPB principles are conducted for systematically varied roadside wall configurations representing distinct propagation conditions. The study constitutes a first controlled experimental step towards characterizing transient, geometry-dependent propagation effects during individual vehicle pass-bys. Its contribution is to provide time-resolved measurement data and an analysis framework for controlled reference cases that can be used to examine whether traffic-noise prediction and auralization models reproduce effects such as shielding, re-exposure, reflection, diffraction, and spectral redistribution.

Results

The results are presented in three parts. First, maximum A-weighted levels are evaluated using an SPB-based approach. Second, one-third-octave band levels are analyzed to investigate spectral differences between the quasi-free-field and two-wall configuration. Third, time-varying metrics and section-wise mean differences are presented using the wall-defined time sections. All reported results are based on the fixed pass-by length described in *Signal processing and analysis*. Receiver position $p = 1$ is used as the quasi-free-field reference, and wall influences are reported as differences relative to this reference. Owing to the limited number of repetitions per condition ($n = 3$), the analysis is restricted to descriptive statistics, and no inferential statistical models are applied.

Maximum A-weighted level as a function of speed

Figure 1 shows the maximum A-weighted sound pressure level $L_{AF,\max}$ as a function of $\log_{10}(v)$ for Vehicle A (blue) and Vehicle B (orange). Linear regressions according to Eq. (3) were fitted for each receiver position p. Each regression was fitted to pooled $L_{AF,\max}$ measurements of both vehicles at the investigated speeds to characterize the overall speed dependence by receiver position. Table 1 lists the fitted coefficients a_p and b_p of the regression model together with the coefficient of determination R^2. In addition to the position-specific regressions (dashed lines), the regression based on measurements from all positions is also shown (solid line).

For receiver positions $p \in \{1, 2, 4\}$, the fitted intercepts a_p span 19.09 to 21.29 dB(A). The corresponding slopes b_p are of similar magnitude, ranging

from 30.08 to 32.85 dB(A)/decade. For $p = 3$, the fitted intercept $a_3 = 24.51$ dB(A) is higher, and the slope $b_3 = 24.77$ dB(A)/decade is lower. The regression based on measurements from all positions yields $a = 20.13$ dB(A) and $b = 31.56$ dB(A)/decade. Coefficients of determination R^2 range from 0.959 to 1.000.

The wall influence on $L_{AF,\max}$ is expressed as mean differences $\Delta\overline{L}^{(p)}_{AF,\max}$ relative to $p = 1$, following Eq. (4). Mean wall influences $\Delta\overline{L}_{AF,\max}$ at 30 and 50 km/h are summarized in Table 2, with the two-wall configuration $p = 3$ highlighted for clarity. Table 2 shows that the largest positive differences occur for Vehicle A at 30 km/h, with $+3.41 \pm 0.04$ dB(A) at $p = 3$ and $+2.67 \pm 0.34$ dB(A) at $p = 4$. For Vehicle A at 50 km/h, all values remain within approximately ±1 dB(A). For Vehicle B, all values remain within approximately ±1 dB(A) at both speeds. At $p = 3$, Vehicle B yields -0.62 ± 0.30 dB(A) at 30 km/h and -0.92 ± 0.41 dB(A) at 50 km/h. The sample standard deviations across repetitions are below 1.36 dB(A) for all reported conditions.

Table 1 | Regression coefficients for the speed-dependent maximum level model

p	a_p in dB(A)	b_p in dB(A)/decade	R^2
1	19.55	32.27	0.962
2	19.09	32.85	0.959
3	24.51	24.77	1.000
4	21.29	30.08	0.997
All positions	20.13	31.56	0.984

Fitted coefficients a_p and b_p, together with the coefficient of determination R^2, are shown for each receiver position p based on pooled measurements from Vehicle A and Vehicle B. The final row shows the regression obtained from all receiver positions.

Table 2 | Mean A-weighted level differences $\Delta\overline{L}^{(p)}_{AF,\max}$ relative to the quasi-free-field reference position $p = 1$ (Eq. (4))

Vehicle	Speed in km/h	$\Delta\overline{L}^{(2)}_{AF,\max}$	$\Delta\overline{L}^{(3)}_{AF,\max}$	$\Delta\overline{L}^{(4)}_{AF,\max}$
A	30	-0.69 ± 0.73	$+3.41 \pm 0.04$	$+2.67 \pm 0.34$
A	50	-0.79 ± 1.36	$+0.61 \pm 0.86$	$+0.25 \pm 0.42$
B	30	$+0.41 \pm 0.61$	-0.62 ± 0.30	$+0.21 \pm 0.23$
B	50	$+0.42 \pm 0.57$	-0.92 ± 0.41	-0.17 ± 0.22

The mean values and standard deviations across repetitions are given in dB(A) (Eq. (5)).

One-third-octave band levels

One-third-octave band sound pressure levels $L(f_c)$ were evaluated for vehicle pass-bys at 30 and 50 km/h. Mean one-third-octave band spectra are shown for $p = 1$ in Fig. 2a and for $p = 3$ in Fig. 2b, corresponding to the quasi-free-field reference and the two-wall configuration, respectively. The results illustrate the frequency-dependent effect of the two-wall configuration. Shaded bands in the figures indicate ±1 sample standard deviation of the band levels at each center frequency f_c across the $n = 3$ repetitions.

The spectra at $p = 1$ in Fig. 2a represent vehicle-specific quasi-free-field baselines while containing the complete vehicle pass-by noise rather than isolated source or propulsion measurements. At 30 km/h, Vehicle A exhibits higher low-frequency levels than Vehicle B, with differences of approximately 11.5 dB(A) at 63 Hz and 5.8 dB(A) at 250 Hz. At $p = 1$, the spectra exhibit a broad maximum in the mid-frequency range, with decreasing levels toward the lower and higher bands. The lowest mean band levels occur in the 50 Hz band, while peak levels are found around 1000 to 1250 Hz. At $p = 3$, the overall spectral shape remains similar to that at $p = 1$, while the two-wall configuration introduces frequency-dependent level changes (Fig. 2b). Across conditions, the highest one-third-octave band levels occur around 1 kHz at both receiver positions, with the exception of Vehicle A at 30 km/h at $p = 3$, where the maximum occurs at 250 Hz. For Vehicle A at 50 km/h at $p = 3$, elevated levels are also observed at 250 Hz, although the overall maximum remains at 1 kHz. Inter-vehicle differences are largest in the low-to-mid-frequency range (approximately 200 to 315 Hz), with peak differences of up to about 15 dB(A) at 250 Hz. At 50 km/h, the spectra of the two vehicles are similar across most frequency bands, whereas at 30 km/h, larger differences persist over a broader mid-frequency range.

At $p = 3$, both vehicles generally exhibit lower sample standard deviations than at $p = 1$, particularly in the low-frequency range. For Vehicle A at 30 km/h, values below 200 Hz decrease from 2.4 to 8.1 dB(A) at $p = 1$ to 0.2 to 2.6 dB(A) at $p = 3$. For Vehicle B, sample standard deviations at $p = 3$ remain mostly below 1 dB(A), with occasional increases up to about 2 dB(A).

To quantify the influence of the two-wall configuration, per-band level differences relative to the quasi-free-field reference position were evaluated according to Eq. (4). Table 3 summarizes these per-band level differences, including both band-averaged statistics and representative values at 250 Hz

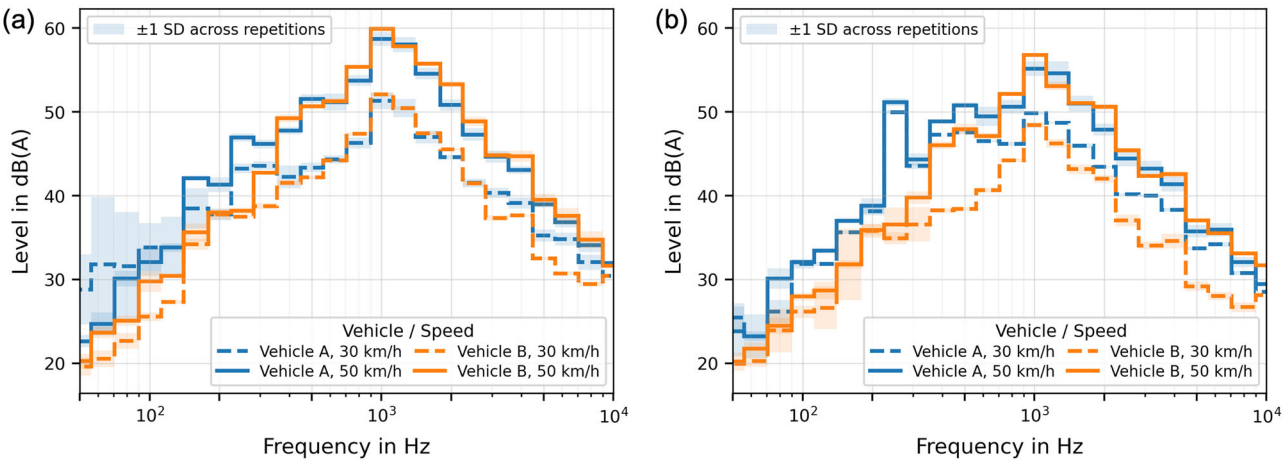


Fig. 2 | One-third-octave band levels for the quasi-free-field and two-wall configurations. Mean band levels are shown from 50 Hz to 10 kHz for Vehicle A in blue and Vehicle B in orange, at 30 km/h with dashed lines and 50 km/h with solid lines. Band levels are shown on a logarithmic frequency axis, with connecting lines used only as visual guides. Shaded bands indicate plus or minus one sample standard deviation across $n = 3$ repetitions. **a** Receiver position $p = 1$, representing the quasi-free-field reference. **b** Receiver position $p = 3$, representing the two-wall configuration.

Table 3 | Per-band level differences between receiver positions $p = 3$ and $p = 1$, computed according to Eq. (4)

Vehicle	Speed in km/h	$\Delta\overline{L}^{(3)} \pm$ SD	$\Delta\overline{L}^{(3)}$(250 Hz) $\pm s_m$	$\Delta\overline{L}^{(3)}$(1 kHz) $\pm s_m$
A	30	−0.8 ± 3.1	+6.7 ± 0.4	−1.4 ± 1.0
A	50	−1.6 ± 2.0	+4.2 ± 0.7	−3.6 ± 1.7
B	30	−2.5 ± 1.6	−2.6 ± 0.8	−3.7 ± 0.1
B	50	−2.5 ± 1.3	−1.9 ± 2.3	−3.1 ± 0.1

Values are reported as the mean ± standard deviation across one-third-octave frequency bands (column 3) and as the mean ± repeatability standard deviation across repetitions at representative frequencies (columns 4 and 5, Eq. (5)); values in dB(A).

and 1 kHz. For all conditions, the band-averaged mean is negative, indicating lower levels at $p = 3$ relative to $p = 1$. The standard deviation across bands ranges between 1.3 and 3.1 dB(A), depending on vehicle and speed, and quantifies the frequency-to-frequency variability of the wall influence across the evaluated bands. The resulting values for $p = 3$ range from −8.6 to +6.7 dB(A) at 30 km/h and from −5.1 to +4.2 dB(A) at 50 km/h, depending on f_c. The largest positive differences occur at low frequencies around 250 Hz for Vehicle A, whereas the most negative differences are observed in the low-to-mid-frequency range from 63 to 160 Hz for Vehicle A and at higher frequencies around 1.25 to 2.5 kHz for Vehicle B. Representative values at 250 Hz and 1 kHz are included in Table 3. These frequencies were selected as representative of characteristic tire–road noise mechanisms, with 250 Hz corresponding to the tire air cavity resonance and 1 kHz representing the mid-frequency range where tire–road interaction noise is typically dominant. At 250 Hz, Vehicle A exhibits positive differences, whereas Vehicle B shows negative differences. At 1 kHz, both vehicles consistently exhibit negative differences.

For completeness, additional one-third-octave band spectra and corresponding tables for the intermediate receiver positions ($p \in \{2, 4\}$) are presented in Supplementary Information under *One-third-octave band levels for receiver positions p = 2 and p = 4*.

Time-varying metrics and section-wise mean differences

Time-varying acoustic metrics were evaluated at receiver positions $p = 3$ and $p = 1$ for both vehicles. Each pass-by event was segmented into five ordered wall-defined time sections (I–V) using the geometric shadow-zone model defined in *Signal processing and analysis* and shown in Fig. 9. Time-series plots of A-weighted level $L_{AF}(t)$, loudness $N(t)$, and sharpness $S(t)$ for the first repetition ($r = 1$) of each vehicle at 50 km/h are shown for position $p = 3$ in Fig. 3 (two-wall configuration) and for $p = 1$ in Fig. 4 (quasi-free-field reference). Corresponding plots for all other combinations of receiver position and vehicle speed are provided in the Supplementary Information under *Time-varying metrics for the remaining evaluated conditions*.

At $p = 3$ (Fig. 3), the presence of the walls introduces clear changes across the wall-defined time sections. For both vehicles, section (III) exhibits the largest means in $L_{AF}(t)$ and $N(t)$ (65.0 dB(A) and 18.7 sone for Vehicle A; 64.9 dB(A) and 16.6 sone for Vehicle B), whereas the shadow-zone sections (II) and (IV) show lower values relative to section (III). In addition, the means decrease again toward section (V) for both vehicles (54.3 dB(A) and 9.5 sone for Vehicle A; 55.1 dB(A) and 9.7 sone for Vehicle B). $S(t)$ shows an increase for both vehicles in section (III) compared with the other sections, with Vehicle B reaching higher $S(t)$ in sections (III) and (V) (1.5 acum and 1.4 acum) than Vehicle A (1.3 acum and 1.1 acum).

By contrast, at $p = 1$ (Fig. 4), the time courses of $L_{AF}(t)$ and $N(t)$ exhibit a single dominant maximum within section (III), with lower values in sections (I) and (V), resulting in an approximately symmetric, unimodal profile with a maximum near the closest point of approach. Vehicle A reaches mean values of 66.7 dB(A) and 19.1 sone in section (III). Vehicle B reaches lower mean values of 66.1 dB(A) and 17.4 sone. For both vehicles, the smallest mean values occur in section (V) (62.2 dB(A) and 13.1 sone for Vehicle A; 63.2 dB(A) and 14.0 sone for Vehicle B). In contrast, $S(t)$ shows only modest variation over the time sections and remains within approximately 1.2 acum to 1.4 acum for both vehicles.

To quantify the trends visible in the time-series plots, section-wise mean metrics were compared between the two-wall configuration ($p = 3$) and the quasi-free-field reference ($p = 1$). Mean differences between receiver positions $p = 3$ and $p = 1$ were evaluated according to Eq. (4) for A-weighted level $\overline{L}_{AF}$, loudness $\overline{N}$, and sharpness $\overline{S}$ as defined in *Signal processing and analysis*. Corresponding standard deviations across repetitions, defined in Eq. (5) as repeatability, were also computed.

Figure 5 presents the section-wise mean differences between the two receiver positions. At 30 km/h (dashed lines), Vehicle A (blue) shows a positive difference in section (III), whereas the shadow-zone sections (II) and (IV) show negative differences. Vehicle B (orange) exhibits negative differences in all five wall-defined time sections (I–V), with the largest difference occurring in the shadow-zone sections (II) and (IV), i.e., $\overline{L}_{AF}$, $\overline{N}$, and $\overline{S}$ at $p = 3$ are lower than or equal to the corresponding values at $p = 1$.

At 50 km/h (solid lines), the largest $\overline{L}_{AF}$ reductions occur in shadow-zone section (II) for both vehicles (Vehicle A: −7.34 dB(A); Vehicle B: −8.03 dB(A)), whereas the reduction in section (III) is approximately zero for Vehicle A and negative for Vehicle B. For $\overline{N}$, Vehicle B exhibits its largest reduction in shadow-zone section (IV) (−6.42 sone), while differences in $\overline{S}$ remain limited across all wall-defined time sections.

At both 30 and 50 km/h, Vehicle A is the only vehicle exhibiting positive differences in $\overline{L}_{AF}$ and $\overline{N}$ in section (III), whereas Vehicle B shows negative differences in these metrics in all five sections (I–V) at both speeds. Results for the intermediate receiver positions ($p \in \{2, 4\}$) are provided in the Supplementary Information under *Section-wise mean differences for receiver positions p = 2 and p = 4*.

Discussion

This study investigated how simplified roadside wall configurations modify low-speed vehicle pass-by noise under controlled SPB-based measurements. As noted in the Introduction, a gap exists between standardized emission-oriented pass-by measurements and the need for controlled data for validating traffic-noise auralizations and numerical propagation models under urban conditions. The present study was designed to address this gap.

Previous work has shown that standardized methods such as the SPB method are well suited to quasi-free-field characterization of vehicle pass-by noise, but they are not intended to capture detailed sound propagation effects caused by nearby urban structures[6,7,15]. By contrast, perceptual and auralization studies have highlighted the importance of sound propagation context, while generally not providing controlled vehicle pass-by measurements with systematically varied urban roadside structures[5,13,14]. The present findings should therefore not be interpreted as contradicting the SPB method, but rather as extending the analysis toward a different research purpose, namely the controlled investigation of urban sound propagation effects.

A direct quantitative comparison with emission and propagation models such as CNOSSOS-EU[8] is not feasible within the present framework, as these models target long-term noise indicators and require additional input parameters such as traffic composition. The present results instead provide controlled pass-by data that isolate shielding and diffraction effects, as well as frequency-dependent redistribution, including section-wise attenuation of up to approximately 8 dB(A), offering a controlled reference that may support evaluation of how such effects are represented in engineering models.

To do this, the study retained key elements of the SPB method, such as constant-speed pass-bys and a quasi-free-field reference position, while using an ISO 10844-compliant pavement[16]. Furthermore, two parallel medium-density fiberboard (MDF) walls were introduced as controlled urban roadside structures. Together with the fixed pass-by length and the geometry-based definition of shadow-zone sections (see Fig. 9), this made it possible to compare conventional level descriptors, spectral measures, and time-varying psychoacoustic metrics within a common framework. This approach links the measurement geometry directly to clearly defined

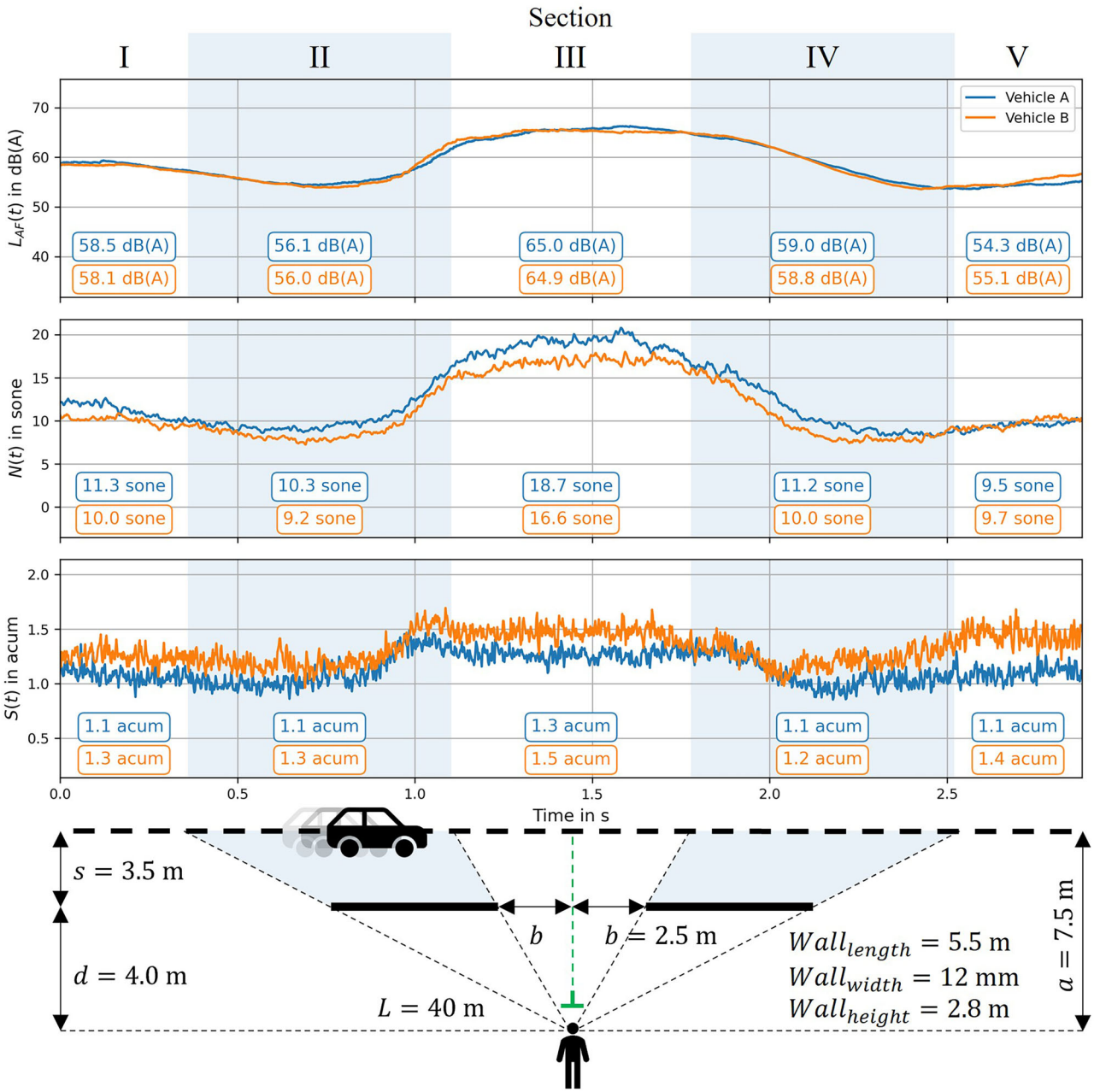


Fig. 3 | Time-varying acoustic metrics for the two-wall configuration. A-weighted level $L_{AF}(t)$, loudness $N(t)$, and sharpness $S(t)$ are shown at 50 km/h for $p = 3$, segmented into the five wall-defined time sections (I–V) according to *Signal processing and analysis*. Shaded regions indicate the shadow-zone sections; section-wise mean metrics for both vehicles are shown at the bottom of each subplot.

temporal sections of the pass-by event. The parallel-wall arrangement does not form an enclosed canyon and therefore limits strong specular reflections. This enables a controlled investigation of diffraction and limited reflection effects without introducing dominant multi-reflection phenomena typical of narrow street canyons. The setup thus represents a simplified proxy for common urban roadside structures such as parked vans or façade segments located between driving lanes and pedestrians. The setup also supports a geometry-based interpretation of direct, diffracted, reflected, and partially transmitted contributions, even though these components were not separated directly in the measurements. Given the surface mass of approximately 9 kg/m^2 for the 12 mm MDF panels[17], sound transmission through the panels is expected to be attenuated according to the mass law, consistent with findings for lightweight barrier configurations[18]; consequently, diffraction at the wall edges is likely to dominate, although this was not quantified explicitly.

A key methodological implication of the present results is that classical SPB method descriptors such as $L_{AF,\max}$ remain useful for pass-by characterization, but they do not fully resolve the geometry-dependent sound propagation effects introduced by urban roadside structures. This is supported by the observation that wall-related differences in $L_{AF,\max}$ are generally small for most tested conditions (Table 2), whereas the section-wise analyses reveal pronounced and repeatable changes in $\overline{L}_{AF}$ and $\overline{N}$ within the shadow-zone sections (Fig. 5). Likewise, the one-third-octave analysis shows frequency-dependent redistribution (Table 3) that is not captured by a single maximum-level descriptor (Fig. 1). Taken together, these findings indicate that time-varying and section-wise evaluations provide complementary information for characterizing urban sound propagation effects beyond what can be inferred from conventional SPB metrics alone.

The results can be summarized in three main points. First, $L_{AF,\max}$ increased approximately linearly with $\log_{10}(v)$ over the investigated speed

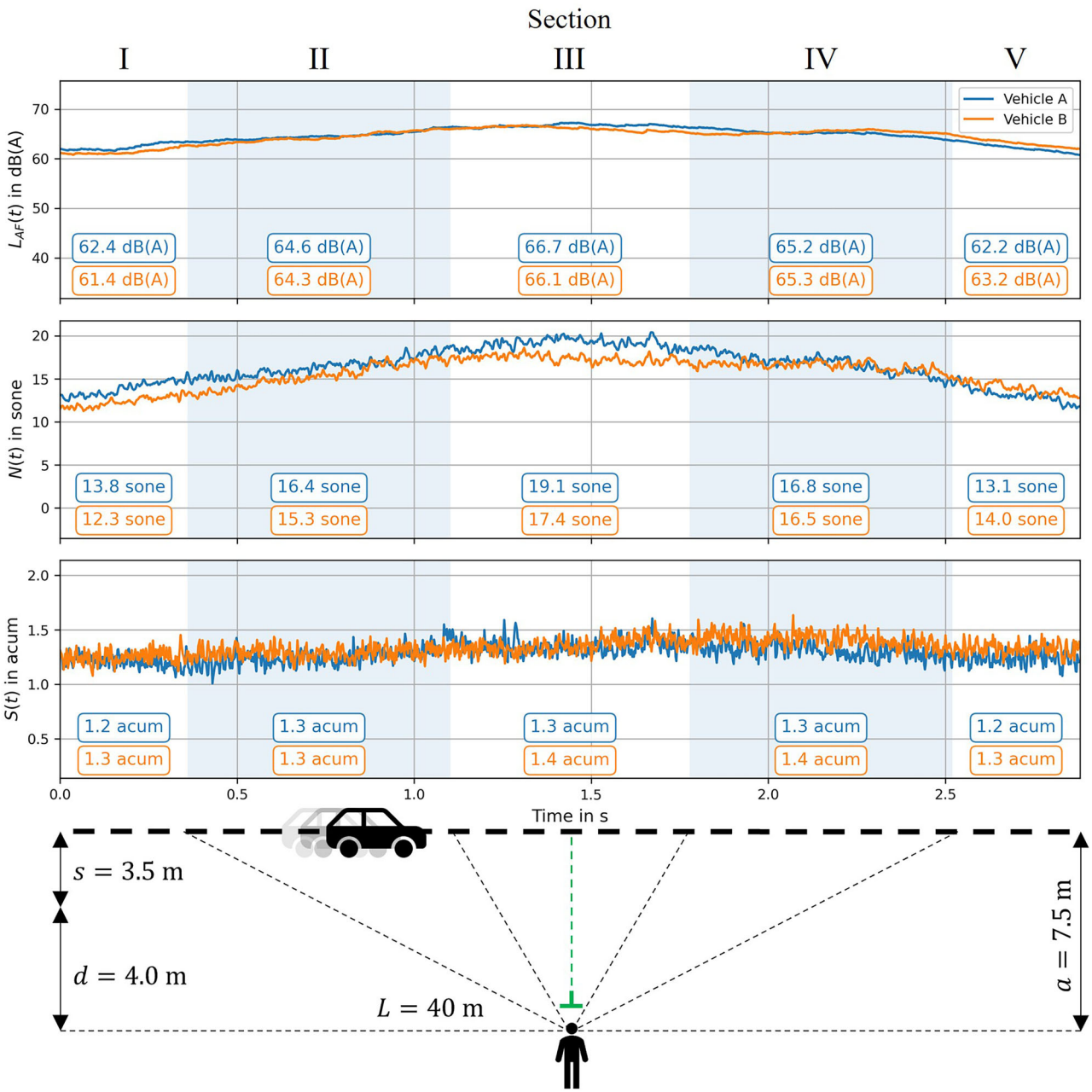


Fig. 4 | Time-varying acoustic metrics for the quasi-free-field reference. A-weighted level $L_{AF}(t)$, loudness $N(t)$, and sharpness $S(t)$ are shown at 50 km/h for p = 1, segmented into the five wall-defined time sections (I–V) according to *Signal processing and analysis*. Shaded regions indicate the shadow-zone sections for comparison; section-wise mean metrics for both vehicles are shown at the bottom of each subplot.

range. The pooled regressions shown in Figure 1 and Table 1 are consistent with this trend for the combined measurements of both vehicles. Second, the one-third-octave analysis showed that the two-wall configuration produced frequency-dependent spectral redistribution rather than a simple broadband increase or decrease. Third, the clearest wall-induced effects appeared in the time-varying and section-wise analyses, where pronounced and repeatable reductions in A-weighted level and loudness occurred mainly in the geometrically defined shadow-zone sections.

The logarithmic formulation was chosen following the SPB evaluation principle, where maximum A-weighted pass-by levels are evaluated as a function of the logarithm of vehicle speed[6]. The approximately linear increase of $L_{AF,\max}$ with $\log_{10}(v)$ is consistent with previous work on tire–pavement interaction noise, which is commonly described by a logarithmic dependence on speed[12,19]. The fitted slopes of approximately 30 to 33 dB(A)/decade for $p \in \{1, 2, 4\}$ (Table 1) fall within the range of roughly 30 to 45 dB(A)/decade reported for tire–road interaction noise[12,19], with typical values for rolling-noise-dominated conditions near the lower end of this range. The lower slope obtained at p = 3 likely reflects the two-wall configuration and associated propagation effects rather than a change in the underlying source mechanism. At the same time, the regressions are empirical and should not be extrapolated beyond the investigated range of 10, 30, and 50 km/h, where more comprehensive emission models are required[8,9,20–22]. A further point to note is that some measurements at 10 km/h were excluded because of external disturbances. For Vehicle A, all measurements at 10 km/h at positions p = 3 and p = 4 were excluded because fan noise contaminated the recordings. For Vehicle B, two measurements at 10 km/h at p = 3 were excluded due to aircraft flyovers. Consequently, the regressions at these positions rely on fewer observations at the lowest speed, which may influence the estimated slope parameters. Nevertheless, the coefficients of determination remain high, indicating that the logarithmic

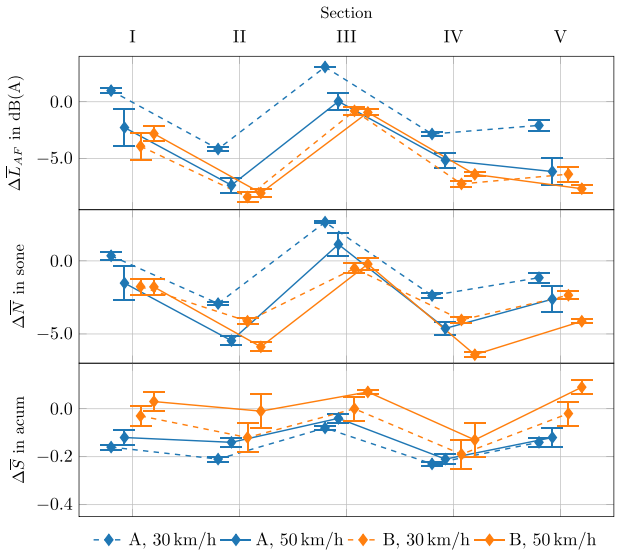


Fig. 5 | Section-wise mean differences computed as $p = 3$ minus $p = 1$ according to Eq. (4) at 30 km/h (dashed) and 50 km/h (solid). Blue denotes Vehicle A and orange denotes Vehicle B. Error bars indicate the standard deviation across repetitions (Eq. (5)).

relation provides a consistent overall description of $L_{AF,\max}$ across the investigated receiver positions, although increased uncertainty at 10 km/h due to background noise may affect the lowest-speed data points.

This interpretation is also consistent with the pass-by geometry. $L_{AF,\max}$ typically occurs near the closest point of approach, where the direct sound path is comparatively less affected by the wall arrangement than in the shadow-zone sections. Accordingly, the main wall-induced effects are expressed more strongly in the temporal and spectral structure of the pass-by event than in the peak value itself. Table 2 shows a vehicle- and speed-dependent pattern in $L_{AF,\max}$: Vehicle A at 30 km/h exhibits larger positive differences at $p = 3$ and $p = 4$, whereas this trend is not observed at 50 km/h or for Vehicle B. Together with the vehicle- and speed-dependent spectral redistribution, this suggests an interaction between vehicle-specific source characteristics and the propagation conditions near the closest point of approach. Since the individual source, reflection, and diffraction contributions were not separated, the underlying cause cannot be determined conclusively. The more general result is therefore not that $L_{AF,\max}$ is insensitive to urban roadside structures, but that it is substantially less sensitive than the section-wise and spectral metrics discussed below.

The spectra at the reference position show a broad mid-frequency maximum around 1000 to 1250 Hz, with comparatively low levels at 50 Hz. Introducing the two-wall configuration did not produce a uniform level shift, but rather changed the balance between frequency components of the vehicles. For Vehicle A, pronounced increases occur around 250 Hz, while decreases are observed at higher frequencies such as 1 kHz. This behavior is consistent with frequency ranges associated with known tire-related mechanisms, such as air-cavity resonance in the range of 200 to 250 Hz and dominant tire–road interaction noise in the mid-frequency range around 1 kHz[10,11]. In contrast, Vehicle B exhibits predominantly negative per-band differences across most frequencies. Consistently, the general band-averaged differences between $p = 3$ and $p = 1$ are negative for all vehicles, indicating an overall reduction of energy in the two-wall configuration despite localized spectral increases. This indicates that the same surrounding geometry can affect the received sound at pedestrian positions differently depending on the vehicle.

The section-wise results provide the strongest evidence for geometry-dependent sound propagation effects. The time-varying analysis shows that effects that are largely hidden in maximum-level metrics become clearly visible once the pass-by is segmented according to the wall-defined time sections, particularly in shadow-zone sections (II) and (IV). At $p = 3$, the pass-by event shows section-dependent variations in level, loudness, and sharpness. By contrast, level and loudness exhibit smooth, unimodal profiles centered around the closest point of approach in section (III) at $p = 1$, while sharpness shows a similar, albeit weaker, trend. This comparatively small variation in sharpness is consistent with traffic-noise research, where perceptual responses are strongly influenced by overall level and loudness, while sharpness represents a timbre-related attribute associated with high-frequency content and becomes more relevant when pronounced spectral differences are present[5,23,24]. The small systematic sharpness differences are also consistent with this interpretation, because they indicate that the observed changes were not primarily associated with pronounced differences in perceptual high-frequency weighting[23,24].

When the source–receiver direct line of sight is obstructed, the received sound pressure level tends to decrease, which is consistent with sound propagation being governed primarily by edge-diffracted sound paths. When the source is located between the walls in section (III), additional diffracted contributions and the ground-reflected component may locally increase the section-wise mean level. This behavior is evident for Vehicle A at 30 km/h, which shows a positive contrast in section (III), while the shadow-zone sections (II) and (IV) exhibit clear attenuation. The positive $L_{AF,\max}$ difference for Vehicle A at 30 km/h in Table 2 is consistent with the positive section-wise difference in section (III) at $p = 3$ shown in Fig. 5. At 50 km/h, the corresponding difference for Vehicle A is approximately zero, whereas Vehicle B shows negative section-wise differences throughout, with the largest reductions occurring consistently in sections (II) and (IV). Hence, the magnitude and sign of wall-induced changes depend not only on geometry but also on vehicle-specific emission characteristics. Across both vehicles and speeds, the largest absolute differences between $p = 3$ and $p = 1$ occurred mainly in the shadow-zone sections (II) and (IV), whereas section (III) showed smaller differences and could even yield local increases. The magnitude of these reductions (up to approximately 8 dB(A)) is consistent with diffraction-dominated attenuation for partial line-of-sight obstruction, consistent with diffraction-related attenuation magnitudes represented in engineering propagation models[8]. The section-wise analysis therefore reveals much more clearly than $L_{AF,\max}$ where during the pass-by the relevant sound propagation effects occur. These findings emphasize that the most relevant wall-induced effects arise during sections of line-of-sight obstruction rather than at the closest point of approach. Consequently, temporal segmentation based on geometric shadowing provides a physically meaningful framework for analyzing the urban sound propagation effects of vehicle pass-by noise.

The present work fits between two areas of research: standardized vehicle-noise assessment and urban sound-propagation analysis. One contribution of the study is that it shows how an SPB measurement design can be extended to capture controlled urban propagation effects. A second contribution is that the geometry-based temporal segmentation provides a physically interpretable way of relating measurement results to sound propagation conditions during the pass-by event. A further novel aspect is the combination of simplified roadside wall configurations with section-wise psychoacoustic evaluation. Although the limited number of vehicles, repetitions, and configurations restricts the generalizability of the quantitative results, the methodology provides controlled reference cases for evaluating existing measurement methods, auralization models, and prediction models. While the quasi-free-field reference serves as a baseline, the wall configurations introduce controlled deviations through line-of-sight obstruction and varying contributions of reflection and diffraction. This makes it possible to assess whether auralization or numerical propagation models capture transient effects such as shielding, re-exposure, and frequency-dependent redistribution during the pass-by event. Taken together, these features provide a structured reference dataset for simplified roadside wall configurations.

These contributions have practical implications. For model validation, the results show that agreement in peak level alone is not sufficient, because a model may reproduce $L_{AF,\max}$ while failing to capture transient shadowing,

re-exposure, and frequency-dependent redistribution during the pass-by event. Validation based solely on peak levels or averaged spectra may therefore overlook perceptually relevant temporal features caused by diffraction and partial shielding at roadside boundaries. For traffic-noise auralization, the findings indicate that perceptually relevant differences may occur in specific sections of the event even when the overall maximum level changes little. More generally, the results support the use of geometry-aware and time-varying descriptors when roadside structures dynamically modify sound exposure. The controlled wall configurations and corresponding section-wise metrics therefore provide a more discriminating reference dataset for assessing whether models reproduce not only overall levels but also the timing and magnitude of propagation effects associated with transient shadowing and re-exposure of the vehicle.

Overall, the results show that simplified roadside wall configurations affect the temporal and spectral structure of vehicle pass-by noise more clearly than they affect $L_{AF,\max}$. In particular, the geometry-based section-wise analysis revealed repeatable reductions in A-weighted level and loudness during line-of-sight obstruction, while the one-third-octave analysis showed frequency-dependent redistribution rather than a uniform broadband level change. These findings demonstrate that conventional peak-level descriptors should be complemented by geometry-aware, time-varying, and spectral metrics when evaluating urban sound propagation effects. The controlled wall configurations therefore provide a simplified reference case for validating whether traffic-noise auralizations and numerical propagation models reproduce transient shielding, diffraction, and re-exposure effects. The non-canyon geometry should be regarded as a baseline for subsequent investigations involving more complex urban configurations.

The findings should, however, be interpreted in light of several limitations that affect the transferability of the results to real urban environments. Only two vehicles were investigated, each with a fixed tire configuration, and all measurements were conducted on one ISO-compliant asphalt surface. The roadside wall configuration was represented by a simplified parallel-wall geometry made of MDF and did not include enclosed street-canyon situations with stronger higher-order reflections. The MDF panels have a comparatively low surface mass and finite dimensions, whereas real building façades are typically more massive and continuous. Accordingly, the present setup captures diffraction and reflection effects under simplified conditions, while higher-order reflections and reverberation effects are not represented. The present geometry should therefore be regarded as a controlled baseline for simplified roadside structures rather than as a complete representation of urban traffic noise propagation. While the observed trends, such as shadow-zone attenuation and frequency-dependent redistribution, are expected to be qualitatively transferable, the absolute magnitudes of the effects may differ in real urban environments with stronger reflective interactions. Measurements at 10 km/h did not consistently satisfy the SPB signal-to-noise requirement and were therefore excluded from the detailed spectral and time-varying analyses. Accordingly, the spectral, time-varying, and section-wise conclusions are restricted to 30 and 50 km/h. This speed range corresponds to conditions where tire–road interaction noise is typically dominant, whereas at lower speeds, propulsion-related noise and background noise contributions may play a larger role, which are not represented in the present results. In addition, the receiver positions were measured sequentially rather than simultaneously, and the measurements do not directly decompose the sound field into isolated direct, reflected, diffracted, and transmitted components.

Future work should extend this approach to more complex urban geometries, especially configurations with stronger reflective interaction such as façade-lined street sections or narrower canyon-like environments. It would also be valuable to include a broader range of vehicles, pavements, wall materials, and speeds, particularly low-speed conditions with improved signal-to-noise ratio. In addition, combining this measurement approach with numerical simulations or multi-receiver arrays could help to examine more explicitly the relative roles of direct sound, diffraction, reflection, and transmission. Such work would show how far the framework introduced here can be generalized and would strengthen its use for validating traffic-noise auralizations and numerical propagation models.

Methods

The methodology combines controlled vehicle pass-by measurements with subsequent signal processing and acoustic analysis to investigate how simplified roadside wall configurations influence vehicle pass-by noise propagation. The experimental design builds on the SPB reference geometry and introduces reproducible roadside wall configurations to represent propagation conditions with varying contributions of direct, reflected, and diffracted sound. *Measurements* describes the measurement setup and experimental conditions, while *Signal processing and analysis* outlines the signal processing and evaluation methods.

Measurements

The experimental design was based on the SPB method (ISO 11819-1:2024)[6], which, among other things, specifies a standardized source–receiver geometry for constant-speed vehicle pass-by measurements. In this context, the SPB method involves the statistical evaluation of multiple vehicle pass-bys, whereas controlled pass-by measurements use selected test vehicles under defined operating conditions. To ensure reproducibility on a standardized road surface, all measurements were conducted on a reference pavement conforming to ISO 10844:1994[16]. In contrast to the ISO 362-1 method[15], which focuses on measurements of accelerating vehicles, the present study maintained constant vehicle speed to exclude acceleration-related acoustic effects. The key modification to the SPB method was the introduction of MDF walls, which created controlled boundary conditions and enabled the study of sound propagation in more realistic urban roadside environments.

Four receiver positions ($p \in \{1, 2, 3, 4\}$) were defined following the SPB reference geometry, each located at a horizontal distance of 7.5 m from the lane center (perpendicular to the driving lane) and at a microphone height of 1.2 m. The four receiver positions were measured sequentially using the same calibrated reference microphone, which was repositioned between configurations. This ensured that all positions were evaluated with the same transducer and acquisition chain, but meant that comparisons between positions were based on separate pass-by events. To account for the resulting run-to-run variability, all measurements for a given vehicle and speed were conducted under stable environmental and operational conditions (same day, road surface, vehicle, tires, and instrumentation). Each combination of vehicle, target speed, wall configuration, and receiver position was repeated three times, and the corresponding standard deviations were reported. Figure 6 shows a plan view of the measurement setup, including the wall configurations and receiver positions. In the coordinate system of Fig. 6, the vehicle moves along the x-axis (driving lane), with $x = 0$ at the receiver position of interest and positive x in the direction of motion. The y-axis is perpendicular to the trajectory, with $y = 0$ at the respective receiver position and positive y directed towards the driving lane.

To emulate typical roadside structures between a driving lane and a sidewalk, two reinforced MDF walls were installed parallel to the driving lane (see Fig. 7a). The walls provide a simplified and controlled abstraction of roadside structures, such as parked high-roof vehicles or façade segments located close to the traffic lane, enabling systematic investigation of reflection and diffraction effects. Each MDF wall measured 5.5 m in length, 2.8 m in height, and 12 mm in thickness. The 12 mm MDF thickness corresponds to a surface mass of approximately 9 kg/m^2, which is within the range reported for lightweight barrier materials[17,18]. The walls were arranged with a separation of 5 m (see Fig. 6). The longitudinal dimensions were chosen on the scale of parallel parking spaces: RASt 06 gives parallel-parking frontage lengths of 5.2 m to 5.7 m, consistent with the 5.5 m wall length and the 5 m separation[25]. The wall height of 2.8 m was selected to represent high roadside obstacles, such as high-roof delivery vehicles or roadside screens, rather than continuous building façades. Receiver position $p = 3$ therefore represents a pedestrian-side receiver behind separated roadside obstacles, not a

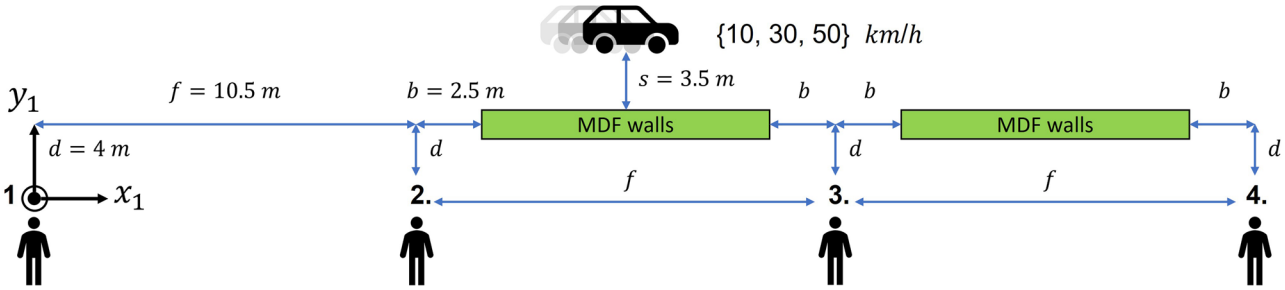


Fig. 6 | Measurement setup and receiver positions. Plan view of the measurement setup showing the driving vehicle, wall configurations, and four receiver positions ($p \in \{1, 2, 3, 4\}$). The coordinate system is defined with the x-axis parallel to the driving lane and the y-axis perpendicular to the driving lane.

Fig. 7 | Test track surface and vehicle pass-by measurement setup. a Vehicle pass-by measurement setup on the ISO 10844-compliant asphalt surface. **b** Aerial view of the ISO 10844-compliant asphalt test surface, shown in light gray. Map data in (**b**): ©OpenStreetMap contributors, licensed under the ODbL, https://www.openstreetmap.org/copyright. The asphalt test surface conforms to ISO 10844:1994[16].

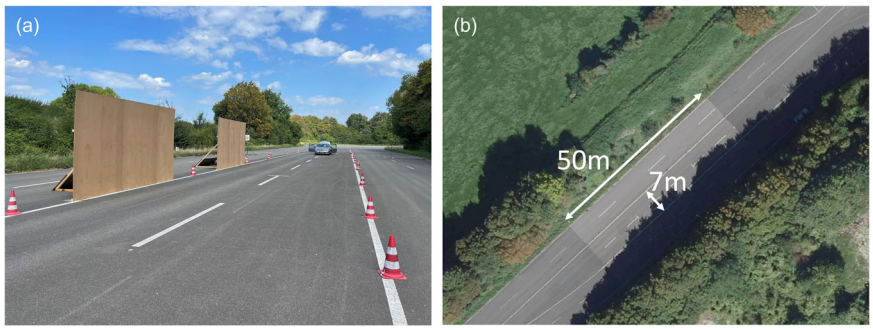
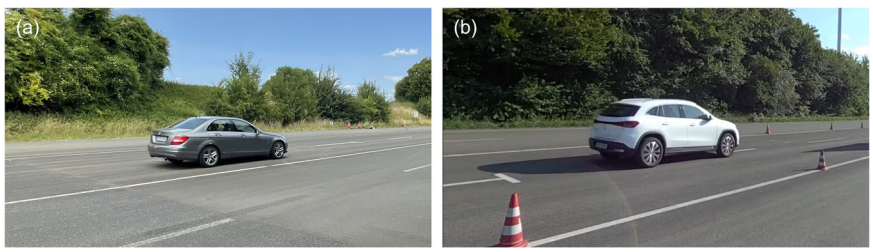


Fig. 8 | Test vehicles used in the measurement campaign. a Vehicle A, a Mercedes W204 C 180 diesel sedan. **b** Vehicle B, a Mercedes EQA 250 battery-electric sport utility vehicle (SUV).



continuous façade case. The inner edges of the walls were located at a lateral distance of 3.5 m from the lane center.

The measurement design aimed to isolate sound propagation differences caused by wall configurations while keeping all other parameters constant. Vehicle speeds of 10, 30, and 50 km/h were selected to cover low, moderate, and typical urban driving speeds within the investigated range. The four receiver positions generated distinct wall-related sound propagation conditions, including a quasi-free-field reference, single-wall configurations, and the two-wall configuration. Within these roadside wall configurations, the shadow-zone sections were defined geometrically based on line-of-sight obstruction between the moving source (vehicle) and the receiver (microphone). These geometric boundary conditions determine when the direct sound propagation path is blocked, such that diffracted propagation is expected to dominate.

The vehicle pass-by measurements were carried out on the ika test track at RWTH Aachen University[26]. Vehicles accelerated before entering the measurement section and then traversed the measurement section at constant speed. All vehicle pass-by events used in this study were recorded exclusively on an asphalt surface conforming to ISO 10844:1994, which is highlighted in light gray in Fig. 7b. The measurement section is located in an open area largely surrounded by agricultural fields and sufficiently far from nearby buildings to minimize additional reflections from surrounding structures, thus conforming to the quasi-free-field conditions required for SPB measurements.

Two passenger vehicles with contrasting propulsion concepts were measured in this study. Vehicle A (see Fig. 8a) was a Mercedes W204 C 180 diesel sedan (D-segment, 4.59 × 1.77 × 1.45m^3) equipped with Michelin Primacy 4 tires (225/45 R17 94Y). Vehicle B (see Fig. 8b) was a Mercedes EQA 250 battery-electric SUV (C-segment, 4.46 × 1.83 × 1.62 m^3) equipped with Continental WinterContact TS 870 P tires (235/55 R18 104V). Vehicle body-type terminology follows ISO 3833[27]. After accelerating in the turning circle, drivers stabilized the target speed using GPS-based speed feedback supported by integrated cruise control in both vehicles. The GPS-based feedback was obtained using a CDG I.1 GPS adapter with a specified speed precision of 0.1 m s^{-1} at 95%[28]. Since continuous speed histories and OBD speed data were not recorded, run-specific speed deviations could not be evaluated retrospectively.

Sound pressure levels were recorded using a Brüel & Kjær 4190 free-field omnidirectional microphone[29]. The omnidirectional microphone was calibrated prior to each measurement session using a Brüel & Kjær Type 4231 acoustic calibrator (Class 1)[30]. Each pass-by event was logged with target speed, receiver position, repetition, and meteorological measurements including air temperature and relative humidity (see Supplementary Information under *Meteorological conditions during pass-by events*). Across the measurement campaign, the ambient air temperature was 28.3 °C ± 1.1 °C, and the relative humidity was 43.3% ± 4.9%. Measurements at 10 km/h did not consistently meet the SPB signal-to-noise-ratio requirement of at least 10 dB(A) above background noise[6]. These measurements

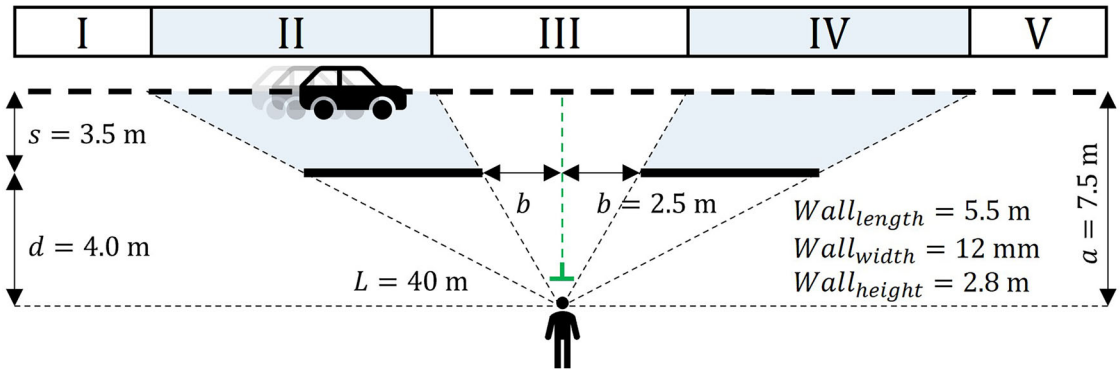


Fig. 9 | Geometric segmentation of the two-wall pass-by configuration. The plan view shows receiver position $p = 3$ and the five ordered wall-defined time sections: (I) Approach, (II) Left shadow zone, (III) Between walls, (IV) Right shadow zone, and (V) Departure.

were nevertheless retained for the analysis of $L_{AF,\max}$ as a function of speed, as they contribute to the characterization of the logarithmic speed dependence. All other analyses were restricted to speeds that consistently fulfill the SPB signal-to-noise criterion.

Signal processing and analysis

For subsequent analysis, all data were restricted to the fixed pass-by length L = 40m centered on the receiver position. This restriction ensures that measurements at $p = 1$ (quasi-free-field reference, i.e., no wall-induced shadow-zone sections) exclude time sections in which the receiver-to-vehicle line of sight would be obstructed by walls associated with the other three receiver positions. Half the pass-by length $L/2$ = 20 m is shorter than the minimum distance from $p = 1$ to the onset of the first shadow-zone section (approximately 21.4 m for Vehicle B, which has the largest overall vehicle dimensions; see *Measurements*), ensuring that all data within the pass-by length remain unobstructed with respect to the wall geometry. The same pass-by length was applied consistently across all vehicles, speeds, positions, and repetitions to ensure comparability of level-based, spectral, and time-varying metric analyses. This restriction is consistent with the SPB method requirement[6] that sound propagation between the vehicle and the microphone is free of reflective or shielding objects.

Tire types were fixed per vehicle, and the road surface was treated as constant[6]. Meteorological conditions were monitored throughout the measurement campaign (see Supplementary Information under *Meteorological conditions during pass-by events*). Air temperature varied only within a narrow range during the measurement campaign (see *Measurements* and Supplementary Information under *Meteorological conditions during pass-by events*), well within the 5 °C range typically considered acceptable for grouped SPB measurements[6]. Temperature corrections specified in the SPB standard were therefore not applied, as the analysis focuses on relative differences between receiver positions and any systematic temperature-related level shift would affect all positions similarly. Accordingly, the observed variations in temperature and humidity are not expected to have a significant influence on the reported level differences or the overall interpretation of the results.

Shadow-zone sections were defined as the wall-defined time sections in which the direct sound path between source and receiver is blocked. Shadow-zone boundaries were derived geometrically based on the intersection of the receiver–source line of sight with the wall edge. Accordingly, the vehicle enters the corresponding shadow-zone section when the receiver–vehicle line of sight intersects the nearest wall edge. For the fixed receiver coordinate y_r, the wall-edge coordinate y_w, and the wall-edge position x_w, the corresponding boundary coordinate is given by

$$x_s = \frac{x_w}{1 - \frac{y_w}{y_r}}. \tag{1}$$

With vehicle speed v and pass-by start position $x_0 = -\frac{L}{2}$, the corresponding time instant is

$$t = \frac{x_s - x_0}{v}. \tag{2}$$

The pass-by event was divided into five ordered wall-defined time sections, as illustrated for the two-wall configuration at $p = 3$ in Fig. 9: (I) Approach, (II) Left shadow zone, (III) Between walls, (IV) Right shadow zone, and (V) Departure. The wall-defined time sections during which the source is geometrically located behind the left and right walls correspond to the shadow-zone sections (II) and (IV), respectively, as determined from Eqs. (1) and (2). All measurements were segmented accordingly for the subsequent time-varying and section-wise analyses.

Results were grouped by experimental condition, defined by the tested vehicle (i), the driving speed (v), and the receiver position (p). In the following, the tuple (i, v, p) denotes a specific condition, where $p \in \{1, 2, 3, 4\}$ refers to the receiver positions shown in Fig. 6. The symbol m is used as a generic placeholder for the evaluated acoustic quantity, such as the maximum A-weighted level $L_{AF,\max}$, the time-varying A-weighted level $L_{AF}(t)$, section-wise mean A-weighted level $\overline{L}_{AF}$, the one-third-octave band level $L(f_c)$ at center frequency f_c, loudness N, or sharpness S.

Regression of $L_{AF,\max}$ versus $\log_{10}(v)$ was performed separately for each p. The dependence was described using the logarithmic model

$$L^{(p)}_{AF,\max}(v) = a_p + b_p \log_{10}(v), \tag{3}$$

where a_p denotes the intercept and b_p the slope parameter for p. Regression of $L_{AF,\max}$ versus $\log_{10}(v)$ was used to describe the speed dependence at each receiver position. Because each fit was based on only three aggregated speed points, the regression was interpreted descriptively.

Mean differences between receiver positions p were evaluated for each metric m as

$$\Delta\overline{m}^{(p)}(i, v) = \overline{m}(i, v, p) - \overline{m}(i, v, 1), \qquad p \in \{2, 3, 4\}, \tag{4}$$

where $\overline{m}(i, v, p)$ denotes the mean value of metric m over the three valid repetitions ($n = 3$) for condition (i, v, p), and $p = 1$ serves as the quasi-free-field reference. Negative $\Delta\overline{m}$ values indicate lower mean metric values at position p than at the reference $p = 1$, whereas positive $\Delta\overline{m}$ values indicate higher ones.

The sample standard deviation of metric m across the n valid repetitions defines the repeatability

$$s_m(i, v, p) = \sqrt{\frac{1}{n-1}\sum_{r=1}^{n}\left(m_r(i, v, p) - \overline{m}(i, v, p)\right)^2}, \tag{5}$$

where $m_r(i, v, p)$ denotes the value of metric m in repetition r for condition (i, v, p), and $\overline{m}(i, v, p) = \frac{1}{n}\sum_{r=1}^{n} m_r(i, v, p)$ is the corresponding mean. For the section-wise comparison tables and plots, values are reported as $\Delta\overline{m}^{(p)}(i, v) \pm s_m(i, v, p)$, where the ± term denotes the repeatability at the comparison position p, defined as the standard deviation of the repeated metric values rather than of per-repetition differences.

All signal processing and metric evaluation follow established international standards to ensure comparability with existing frameworks for measuring and evaluating traffic noise. Time-varying A-weighted sound pressure level $L_{AF}(t)$ was computed using A-weighting and FAST time weighting in accordance with IEC 61672-1[31], consistent with the SPB definition of time weighting F[6]. Maximum A-weighted sound pressure levels, denoted $L_{AF,\max}$, were obtained as the maximum of $L_{AF}(t)$ over the pass-by length L. Time-varying loudness $N(t)$ was computed according to ISO 532-1:2017 using the Zwicker method, and time-varying sharpness $S(t)$ for non-stationary signals was computed according to DIN 45692:2009[24,32]. Loudness and sharpness calculations were implemented using the MOSQITO sound quality library (version 1.2.1)[33].

For the analysis of $L_{AF,\max}$ versus $\log_{10}(v)$ and of one-third-octave band levels $L(f_c)$, the signals were bandpass-filtered from 50 to 10,000 Hz prior to the level evaluation. This range lies within the frequency region typically considered in SPB-based road traffic noise assessments[6]. Except for the results for $L_{AF,\max}$ (Maximum A-weighted level as a function of speed), all measurements at 10 km/h were excluded from the analyses because the SPB signal-to-noise-ratio requirement was not met (see *Measurements*).

For spectral analysis, A-weighted time signals were decomposed into one-third-octave bands using IEC 61260-1-compliant filters[34]. Per-band sound pressure levels were computed as root mean square values over the pass-by length. Band levels were averaged across repetitions and reported as mean values with corresponding sample standard deviations. The analysis was restricted to positions $p \in \{1, 3\}$ to contrast the quasi-free-field configuration with the two-wall configuration.

Additional analyses were performed to examine time-varying sound propagation effects induced by the wall configurations during the pass-by event. Positions $p \in \{2, 4\}$ were excluded from these analyses, as they represent partial subsets of the two-wall configuration at $p = 3$ and therefore do not span the full set of wall-defined time sections within the pass-by length. For each pass-by event condition, the first repetition ($r = 1$) was selected for time-series plots of the time-varying metrics.

Section-wise mean values of L_{AF}, loudness N, and sharpness S were computed for each repetition at $p \in \{1, 3\}$ across the five ordered wall-defined time sections shown in Fig. 9. Differences were aggregated across repetitions and reported as mean values with corresponding sample standard deviations.

Data availability

The data that support the findings of this study are openly available in the Zenodo repository at https://doi.org/10.5281/zenodo.21469910.

Received: 22 April 2026; Accepted: 18 August 2026;
Published online: 06 October 2026

References

1. World Health Organization, Regional Office for Europe. *Environmental Noise Guidelines for the European Region*. https://www.who.int/europe/publications/i/item/9789289053563 (World Health Organization, Regional Office for Europe, 2018).
2. United Nations, Population Division, World Bank & Our World in Data. *Urban Population (% of Total Population)*. https://ourworldindata.org/urbanization. Data compiled from UN World Urbanization Prospects and World Bank World Development Indicators (2024).
3. Bundesministerium für Umwelt, Naturschutz, Bau und Reaktorsicherheit & Umweltbundesamt. *Umweltbewusstsein in Deutschland 2016: Ergebnisse einer repräsentativen Bevölkerungsumfrage*. Tech. Rep., Umweltbundesamt, Dessau-Roßlau. https://www.umweltbundesamt.de/publikationen/umweltbewusstsein-in-deutschland-2016. Research project no. 3715 16 103 0 (2017).
4. Erraji, A., Stienen, J. & Vorländer, M. The image edge model. *Acta Acust.* **5**, 17 (2021).
5. Oehme, A. et al. A measuring instrument for the perceptual dimensions of road traffic noise. *J. Acoust. Soc. Am.* **157**, 1587–1597 (2025).
6. Deutsches Institut für Normung. *DIN EN ISO 11819-1:2024-10 Acoustics – Measurement of the Influence of Road Surfaces on Traffic Noise – Part 1: Statistical Pass-by Method (ISO 11819-1:2023)*. German adoption of an International Standard (Deutsches Institut für Normung, 2024).
7. International Organization for Standardization. *ISO 11819-2:2017 Acoustics – Measurement of the Influence Of Road Surfaces on Traffic Noise – Part 2: The Close-proximity Method*. International Standard (International Organization for Standardization, 2017).
8. Kephalopoulos, S., Paviotti, M. & Anfosso-Lédée, F. *Common Noise Assessment Methods in Europe (CNOSSOS-EU)*. Tech. Rep. EUR 25379 EN (Publications Office of the European Union, Luxembourg, 2012).
9. European Commission. Commission directive (EU) 2015/996 of 19 May 2015 establishing common noise assessment methods according to directive 2002/49/EC (text with EEA relevance). *Off. J. Eur. Union* 1–823. http://data.europa.eu/eli/dir/2015/996/oj (2015).
10. Blom, R. *Report on Tyre/Road Noise: Generation Mechanisms, Influence of Tyre Parameters and Experiment on Belt Resonances*. Tech. Rep. DCT 2004.020 (Technische Universiteit Eindhoven, 2004).
11. Kropp, W., Larsson, K., Wullens, F. & Höstmad, P. B. U. Tyre/road noise generation – modelling and understanding. In *Proc. Spring Meeting of the Institute of Acoustics* (Institute of Acoustics, 2004).
12. Li, T. Influencing parameters on tire–pavement interaction noise: Review, experiments, and design considerations. *Designs* **2**, 38 (2018).
13. Georgiou, F., Hornikx, M. & Kohlrausch, A. Auralization of a car pass-by using impulse responses computed with a wave-based method. *Acta Acust. U. Acust.* **105**, 381–391 (2019).
14. Georgiou, F., Hornikx, M. & Kohlrausch, A. Auralization of a car pass-by inside an urban canyon using measured impulse responses. *Appl. Acoust.* **183**, 108291 (2021).
15. International Organization for Standardization. *ISO 362-1:2022 Acoustics – Engineering Method for Measurement of Noise Emitted by Accelerating Road Vehicles – Part 1: M and N Categories*. International Standard (International Organization for Standardization, 2022).
16. International Organization for Standardization. *ISO 10844:1994 Acoustics – Specification of Test Tracks for the Purpose of Measuring Noise Emitted by Road Vehicles*. International Standard (withdrawn). Withdrawn; replaced by ISO 10844:2011 and ISO 10844:2021 (International Organization for Standardization, 1994).
17. Peeters, F., Peeters, B. & Wijnant, Y. Determination of acoustic properties of noise barriers. In *Proc. Fortschritte der Akustik – DAGA 2016*, 798–801. https://pub.dega-akustik.de/DAGA_2016/data/articles/000119.pdf (2016).
18. Chen, K. & Beresford, T. Lightweight noise barriers: the real-world effects of panel surface mass and absorption on acoustic performance. In *Proc. Acoustics 2019: Moving Forward with Acoustics*, 607–614 (Australian Acoustical Society, Cape Schanck, Victoria, Australia, 2019).
19. Li, T. A review on physical mechanisms of tire–pavement interaction noise. *SAE Int. J. Veh. Dyn. Stab. NVH* **3**, 87–112 (2019).
20. Jonasson, H. G. *Nord2000 (2006): Acoustic Source Modeling of Nordic road vehicles*. Tech. Rep. SP Report 2006:12 (SP Swedish National Testing and Research Institute, 2006).
21. Jonasson, H. et al. *Source modelling of road vehicles*. Deliverable 9 of the HARMONOISE Project, Technical Report HAR11TR-041210-

SP10 (SP Swedish National Testing and Research Institute, Borås, Sweden, 2004).
22. Sakamoto, S. Road traffic noise prediction model "ASJ RTN-Model 2018": report of the research committee on road traffic noise. *Acoust. Sci. Technol.* **41**, 529–589 (2020).
23. Fastl, H. & Zwicker, E. Sharpness and sensory pleasantness. In *Psychoacoustics: Facts and Models*, 3rd edn, 239–246 (Springer, 2007).
24. Deutsches Institut für Normung. DIN 45692:2009 *Measurement Technique for the Simulation of the Auditory Sensation of Sharpness*. German Standard (Deutsches Institut für Normung, 2009).
25. Forschungsgesellschaft für Straßen- und Verkehrswesen. *Directives for the Design of Urban Roads (RASt)*. Edition 2006, Translation 2012, FGSV No. 200 E (FGSV Verlag, Cologne, 2012).
26. Institut für Kraftfahrzeuge (ika), RWTH Aachen University. ika-teststrecke. https://www.ika.rwth-aachen.de/de/kompetenzen/ausstattung/infrastruktur/ika-teststrecke.html.
27. International Organization for Standardization. *ISO 3833:2022 Road Vehicles – Types – Terms and Definitions*. International Standard (International Organization for Standardization, 2022).
28. HEAD acoustics GmbH. CDG I.1 (Code 3796): GPS Adapter (Data Sheet). https://cdn.head-acoustics.com/fileadmin/data/en/Data-Sheets/Accessories/CDG-1.1-GPS-Adapter-3796-Data-Sheet.pdf (2016).
29. Brüel, H. & Kjær. Type 4190: 1/2-inch free-field microphone (product data sheet). https://www.bksv.com/doc/bp2211.pdf.
30. Brüel, H. & Kjær. Type 4231: Acoustic calibrator (product data sheet). https://www.bksv.com/media/doc/bp1311.pdf.
31. International Electrotechnical Commission. *IEC 61672-1:2013 Electroacoustics – Sound Level Meters – Part 1: Specifications. International Standard. Time weighting F (FAST) with Time Constant τ = 125 ms* (International Electrotechnical Commission, 2013).
32. International Organization for Standardization. *ISO 532-1:2017 Acoustics – Methods for Calculating Loudness – Part 1: Zwicker Method*. International Standard (International Organization for Standardization, 2017).
33. Green Forge Coop. MOSQITO, version 1.2.1 [Computer software]. https://doi.org/10.5281/zenodo.11026796 (2024).
34. International Electrotechnical Commission. *IEC 61260-1:2014 Electroacoustics – Octave-band And Fractional-octave-band Filters – Part 1: Specifications*. International Standard (International Electrotechnical Commission, 2014).

Acknowledgements

This work was conducted as part of the "BaLSaM" research project, funded by the Federal Ministry for Digital and Transport on the basis of a decision by the German Bundestag (funding reference: 01FV2043A). The authors thank the project partners: the Institute for Automotive Engineering at RWTH Aachen University, HEAD acoustics GmbH, and REICHER HAASE ASSOZIIERTE GmbH. The funder had no role in the study design, data collection and analysis, interpretation of the results, or preparation of the manuscript.

Author contributions

C.M., L.A. and J.F. conceptualized the study, developed the methodology, interpreted the results, and reviewed and edited the manuscript. C.M. and L.A. designed the experimental setup. C.M. conducted the measurements, curated the data, performed the formal analysis, and wrote the original manuscript. L.A. and J.F. provided resources and acquired funding. J.F. supervised the work and managed the project. All authors reviewed and approved the submitted version of the manuscript.

Competing interests

The authors declare no competing interests.

Additional information

Supplementary information The online version contains supplementary material available at https://doi.org/10.1038/s44384-026-00077-2.

Correspondence and requests for materials should be addressed to Chalotorn Möhlmann.

Reprints and permissions information is available at http://www.nature.com/reprints

Publisher's note Springer Nature remains neutral with regard to jurisdictional claims in published maps and institutional affiliations.

Open Access This article is licensed under a Creative Commons Attribution 4.0 International License, which permits use, sharing, adaptation, distribution and reproduction in any medium or format, as long as you give appropriate credit to the original author(s) and the source, provide a link to the Creative Commons licence, and indicate if changes were made. The images or other third party material in this article are included in the article's Creative Commons licence, unless indicated otherwise in a credit line to the material. If material is not included in the article's Creative Commons licence and your intended use is not permitted by statutory regulation or exceeds the permitted use, you will need to obtain permission directly from the copyright holder. To view a copy of this licence, visit http://creativecommons.org/licenses/by/4.0/.

© The Author(s) 2026